

Accelerating Battery Manufacturing Optimization by Combining Experiments, *In Silico* Electrodes Generation and Machine Learning

*Marc Duquesnoy,^{1,2} Teo Lombardo,^{1,2} Mehdi Chouchane,^{1,2} Emiliano N. Primo,^{1,2} Alejandro A.
Franco^{1, 2, 3, 4, *}*

¹ Laboratoire de Réactivité et Chimie des Solides (LRCS), UMR CNRS 7314, Université de Picardie Jules
Verne, Hub de l'Energie, 15, rue Baudelocque, 80039 Amiens Cedex, France

² Réseau sur le Stockage Electrochimique de l'Energie (RS2E), FR CNRS 3459, Hub de l'Energie, 15, rue
Baudelocque, 80039 Amiens Cedex, France

³ ALISTORE-European Research Institute, FR CNRS 3104, Hub de l'Energie, 15, rue Baudelocque, 80039
Amiens Cedex, France

⁴ Institut Universitaire de France, 103 Boulevard Saint Michel, 75005 Paris, France

* corresponding author: alejandro.franco@u-picardie.fr

ABSTRACT

Both the society and the market calls for safer, high-performing and cheap Li-ion batteries (LIBs) in order to speed up the transition from oil-based to electric-based economy. One critical aspect to be taken into account in this modern challenge is LIBs manufacturing process, whose optimization is time and resources consuming due to the several interdependent physicochemical mechanisms involved. In order to tackle rapidly this challenge, digital tools able to accelerate LIBs manufacturing optimization are crucially needed for both well assessed and recently discovered chemistries. The methodology presented here encompasses experimental characterizations, *in silico* generation of electrode mesostructures and machine learning algorithms to track the effect of manufacturing over a wide array of mesoscale electrode properties critically linked to the electrochemical performance. Particularly, features as the interconnectivity of the particles network, the electrolyte tortuosity and effective ionic conductivity, the percentage of current collector surface covered by either active material or carbon-binder domain particles and the active material surface in contact with electrolyte were analysed and discussed in detail. This approach was tested and validated for the case of $\text{LiNi}_{1/3}\text{Mn}_{1/3}\text{Co}_{1/3}\text{O}_2$ -based cathodes calendaring, proving its capability to ease the process parameters-electrode properties interdependencies analysis, paving the way to deeper understanding and then faster optimization of LIBs manufacturing

KEYWORDS

Li-ion batteries, manufacturing, machine learning, electrodes mesostructure, calendaring.

1. INTRODUCTION

Since the beginning of human History, and particularly in the last two centuries, we have facilitated our life by designing tools, improving them and accelerating their production. This innate characteristic led us to shape our environment and develop our societies. However, it is now imperative to face the challenges arising from two centuries powered by oil-based resources, for which a transition to massive use of sustainable energies have to be urgently addressed. To answer to these concerns, the demand on energy storage technologies research compels the scientific community to develop new tools capable of accelerating R&D. The last thirty years have shown that Li-ion batteries (LIBs) are the most suited technology to move from an oil-based to an electrical-based society.¹⁻⁵ However, their performance, durability, recyclability and CO₂ fingerprint require further improvement to make feasible this transition. This can be achieved thanks to materials design,⁶⁻⁸ innovative manufacturing⁹⁻¹¹ and manufacturing optimization,¹²⁻¹⁴ or most likely, thanks to a combination of all of them. Regarding the latter, both experimental and modelling approaches can be used to carry out its optimization.¹⁵⁻²⁴ Particularly, the experimental approach is the one that has mainly driven LIBs improvements, by unravelling links between the manufacturing parameters and the electrochemical performance, upon others.¹⁵⁻¹⁷ However, it heavily relies on trial and error, which is highly inefficient in terms of time, cost and resources.

The manufacturing optimization is a complex multi-variable problem for which different scales are involved, namely interfaces at the nanoscale, particles at the microscale, particles aggregates at the mesoscale and cell components at the macroscale. To tackle such a complex scenario, a complete understanding of all the parameters involved in all of these scales is needed. As recently pointed out by Rynne *et al.*, design of experiments (DoE) can be used to minimize the number of experiments to perform and to derive mathematical models describing the relationships between the parameters analysed and the observable(s) of interest, through statistical analysis.^{20,21} However, these empirical mathematical models were limited to linear or quadratic relationships, which could not be enough to capture the expected complex relationships between manufacturing parameters and electrode properties at the different scales. Moreover, some of these properties (as the active material

(AM) surface in contact with the electrolyte) are extremely difficult to measure routinely at the experimental level. In this sense, an experimentally validated mesoscale (tens of μm) physical model can easily give access to these properties, allowing a deeper understanding of the system under analysis. The importance of physicochemical 3D mesoscale models then starts to be recognized.^{22–31} Nonetheless, with the currently available hardware technology, they can still be computationally too expensive for their systematic use in experimental data analysis.

The described scenario calls for faster approaches combining experiments and models. The blooming Artificial Intelligence (AI) field promises to accelerate the manufacturing optimization by revealing patterns hardly recognizable by “classical” analysis methods.^{14,32–37} As they do not rely on physical models, the feasibility of this approach depends on the capability to generate high quality datasets (from experiments, physical models or both of them simultaneously) complete enough to describe the battery manufacturing, which most likely represents the limiting step to develop AI models. Takagishi *et al.* recently reported a machine learning (ML) approach in which the datasets were built by randomly generating *in silico* electrode mesostructures composed of only AM particles coupled with a zero-dimensional electrochemical model to calculate the charge/discharge specific resistance.³⁸ Even if the above-mentioned approach allows to build rapidly a large dataset (2000 electrode mesostructures), its main drawbacks are the complete lack of link between the generated electrode mesostructures and the experimental manufacturing conditions, as well as the concerns about the reliability of the randomly generated electrode mesostructures. Furthermore, the approach reported by these authors does not consider the carbon-binder domain (CBD), whose heterogeneous distribution throughout the electrode was demonstrated to have a major importance in the performance of LIBs.^{27,28,39}

ML algorithms combined with experimental data were recently proved by us to be suitable for discovering and assessing the interdependencies between manufacturing parameters and electrode properties for the case of electrode slurry features and coating conditions.³² An ideal strategy for a systematic use of ML-based approaches should combine the intrinsic reliability of experiments and physics-based modelling with the high throughput of stochastically generated electrodes. This work aims to introduce a novel methodology (Figure 1), hereafter called *hybrid methodology*, encompassing experiments

and/or physics-based modelling together with data-driven electrode mesostructures generation and ML algorithms to speed up manufacturing optimization of either well-known or novel LIBs chemistries. The hybrid methodology relies on results coming from experiments or physics-based modelling to investigate the effects of manufacturing variables on electrodes properties (Figures 1A). The found trends can be expressed through equations arising from mathematical fitting or from ML models, which are then embedded into a data-driven electrode mesostructure generator (Figure 1B). The latter means that some features of the electrode mesostructure, as the evolution of the electrode thickness/porosity along calendaring or the particles reorganization along solvent evaporation, can be controlled through the experimental or computational inputs, while the remaining mesostructure features are defined by a stochastic algorithm. The so-generated electrode mesostructures can then be analysed in terms of several electrode properties critically impacting electrochemical performance, such as the particles interconnectivity or the electrolyte effective conductivity (Figure 1C). Moreover, the low computational cost of the data-driven electrode mesostructure generator allows investigating broad arrays of conditions and electrode properties, offering a broader view on the manufacturing process under analysis. These data can then be processed through ML algorithms in order to develop human interpretable graphs mapping the effect of electrode and process variables on the electrode properties through regression or classification (Figure 1D).

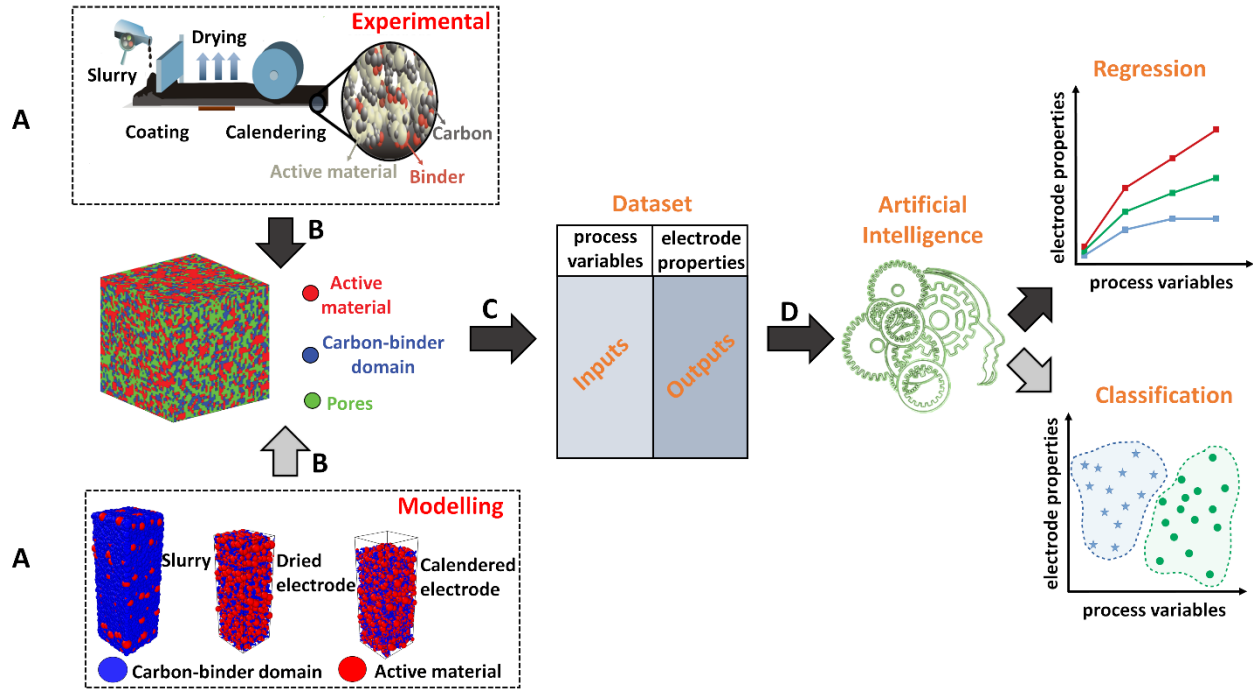


Figure 1. Overall workflow of the hybrid methodology presented in this work. Experimental and/or physics-based computational results capturing the impact of manufacturing parameters on electrode mesostructure properties (A) are used in a data-driven stochastic electrode mesostructure generator algorithm (B) that calculates the electrode mesostructure properties associated to the manufacturing conditions analysed, building the dataset (C). Such dataset is used to train and validate ML algorithms allowing to map and identify the interdependencies between electrode properties prior the manufacturing step under analysis, process parameters (reported in the Figure as process variables) and electrode properties after the manufacturing process investigated (D). Dark grey arrows represent the steps considered along this work, while light grey ones indicate future perspectives of this methodology.

While the effect of manufacturing on macroscopic electrode properties (as its porosity, thickness and mass loading) can be easily captured experimentally, the evolution of mesoscale properties can be studied through experimentally validated physics-based modelling. As extensively demonstrated by us in previous publications, 3D physics-based models offer critical mesoscale information, as the evolution of the percentage of AM surface in contact with the electrolyte or the spatial particles organization through radial

distribution function analysis.²⁶⁻³⁰ What is more, the same approach presented here could be developed by using tomography images as inputs for the analysis. Regardless their high cost in terms of time and resources, hampering their routinely implementation, a recent work by Gayon-Lombardo *et al.*⁴⁰, reporting a ML algorithm trained with tomography images and capable of reconstructing reliable electrode mesostructures, opens the door for embedding tomography-like structures in the overall methodology presented above.

In this work we present a first case study analysed through our hybrid methodology encompassing experimental data, data-driven electrode mesostructures generation and ML. Particularly, this methodology was tested and validated for the case of $\text{LiNi}_{1/3}\text{Mn}_{1/3}\text{Co}_{1/3}\text{O}_2$ -based cathodes by analysing the effect of calendaring pressure, initial electrode porosity and composition on electrode properties such as the solid and liquid phases tortuosities (τ), electrolyte effective conductivity, percentage of current collector (CC) covered by AM or CBD phases and percentage of AM surface in contact with the electrolyte. For the sake of clarity, the demonstration carried out along this work does not include physical modelling as input in the computational workflow, aspect that is being developed in our team and that will be integrated in later publications by us.

2. COMPUTATIONAL AND EXPERIMENTAL METHODS

2.1. Computational methodology

The workflow used along this work constitutes a part of the overall methodology presented above (cf. Figure 1), and it is schematized in Figure 2. First, experimental results are used to determine the relationship between the porosity after the calendaring (ε_{cal}) in terms of the electrodes properties prior the calendaring (its composition, porosity (ε_{init}) and thickness) and the process parameter (calender pressure). An experimental dataset of 66 electrodes encompassing 14 different initial/calendering conditions was constructed. Afterwards, a polynomial fitting of these results is performed to mathematically link ε_{cal} to the electrode properties and the process parameter analysed (Figure 2A). The accuracy

of the fitted model is of ~97%, as discussed in more detail in Section S1 in the Supporting Information.

The equation found through the above-mentioned fitting was implemented in an *in house* data-driven electrode mesostructure generator based on Matlab[®] programming language (Figure 2B). Starting from a fixed initial simulation box ($x \times y \times z$, $50 \times 50 \times 100 \mu\text{m}^3$), and as a function of the calendaring conditions chosen, the electrode porosity and thickness (z dimension) after the calendaring are calculated through interpolation of the mathematical expression derived in the previous step, allowing to rapidly build larger datasets respect the experimental one. The x and y dimensions were maintained constant. Afterwards, the new simulation box is filled stochastically with AM and CBD phases based on the electrode composition and the experimental AM particle size distribution, as it can be seen in the representative electrode mesostructures for different AM compositions shown in Figure 3. More details on the electrodes generation based on the stochastic procedure can be found in Section S3, in the Supporting Information.

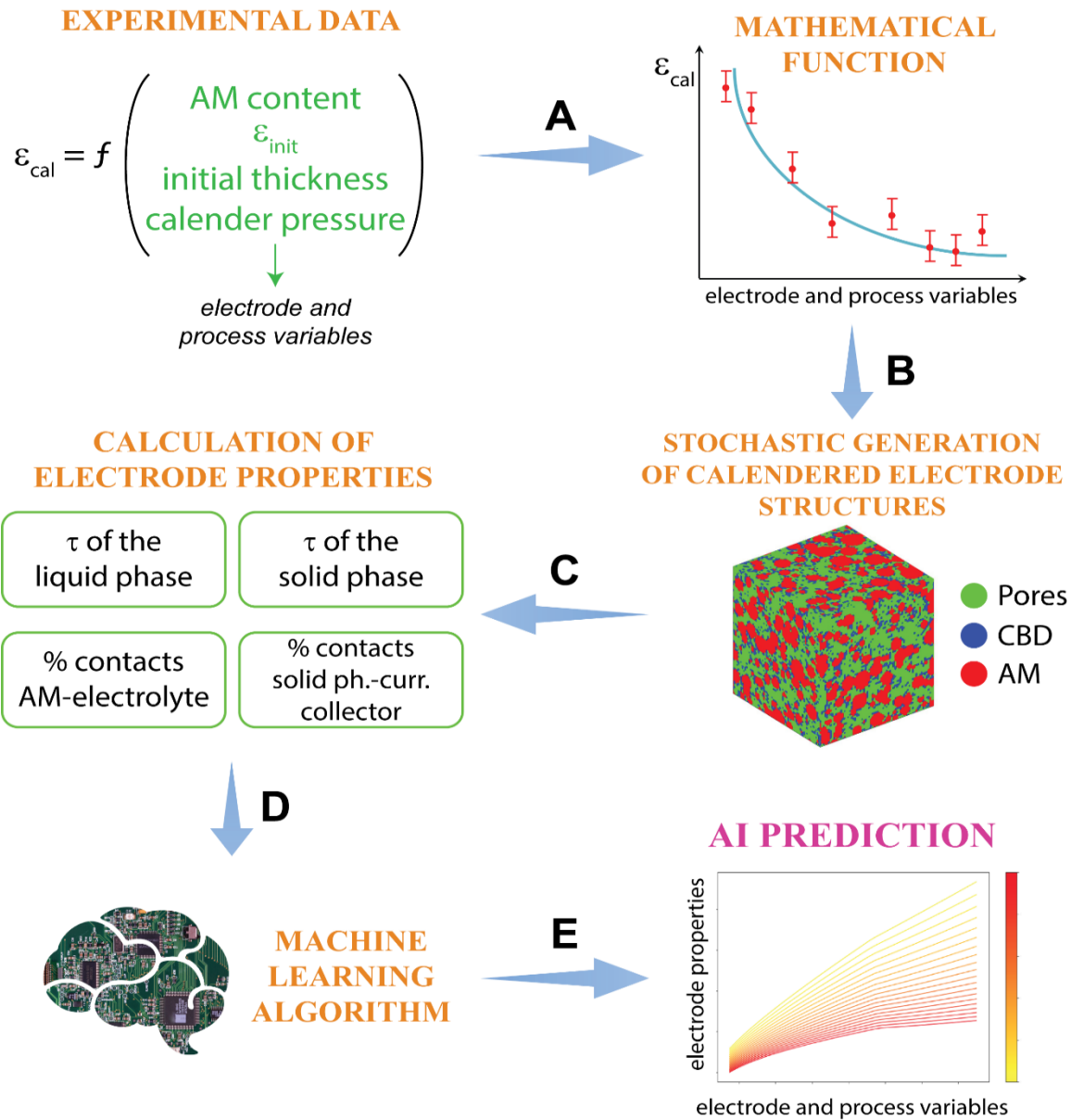


Figure 2. The hybrid methodology workflow implemented in this work. Experimental data is used to develop a mathematical equation (A), which is then embedded into a data-driven stochastic electrode generator (B) that calculates the electrode mesostructure properties associated to different process conditions (C). The developed dataset is used to train and validate the ML algorithm (D) which allows to map and identify the interdependencies between electrode properties prior the manufacturing, process parameters (reported in the Figure as electrode and process variables) and electrode properties after the manufacturing process investigated (E).

The generated electrode mesostructures are then analysed in terms of their liquid-phase and solid-phase τ (through TauFactor⁴¹), percentage of current collector (CC) surface covered by AM or CBD phase (%_{CC-AM} or %_{CC-CBD}, respectively) and percentage of AM surface covered by the electrolyte, referred thereafter as active surface (Figure 2C). Herein, all the void space in the electrode mesostructure is considered to be filled with electrolyte.⁴² Due to the stochastic nature of the generated electrode mesostructures, this procedure is repeated ten times for each calendaring condition and the average values constitute the dataset used by the ML algorithms (4400 structures hence 440 data points). The aim of the latter is to build electrode and process variables-electrode properties interdependencies “maps”, in order to ease their identification and understanding. For the development of ML models (Figure 2D and E) two algorithms were tested, namely Deep Neural Network (DNN)⁴³ and Sure Independent Screening and Sparsifying Operator (SISSO)⁴⁴, using as training and test sets constituted of randomly selected 80% and 20% of the dataset, respectively. The latter allows to reach higher prediction accuracies, and it was then selected for this work. Ouyang *et al.*⁴⁴ recently developed the SISSO algorithm, which relies on identifying descriptors defined as non-linear combinations of the original model inputs upon billions of possibilities, where the chosen ones minimize the model error. This data-driven approach relies on training and test/validation procedures onto the dataset to identify these descriptors, which ranks it as a ML algorithm. SISSO has two main advantages when compared with other ML methods: (i) it outputs a mathematical equation describing the relations between input(s) and output(s), and (ii) it gives reliable results even with relatively small training datasets. (i) allows to analyse the physical meaning of the model developed and to generalize it to other similar case studies, while (ii) reduces the time and cost needed to build the dataset. Further details of the implementation of the SISSO algorithm, including all the equations obtained, are reported in Section S4 in the Supporting Information. The predictive accuracy of the models obtained from DNN and SISSO was assessed by using their test sets through regression plots (true values vs. predicted values) for all the electrode properties examined, as reported in Section S5 together with the training and test sets selection procedure. These plots allow to compare the predictions obtained by the ML

model with the values coming from the test dataset. Moreover, a validation dataset composed of 440 data points (not considered in both training and test sets) was used to further validate the models obtained using the SISO method. The prediction accuracy for the test and validation analysis was always higher than 97%, except for $\%_{CC-AM}$, whose prediction accuracy is of $\sim 76\%$. The latter is understandable, considering the dimension of AM particles ($\sim 3-10 \mu\text{m}$) and the relatively small surface area of the CC ($50 \times 50 \mu\text{m}^2$). Therefore, even slight changes in the number of AM particles in contact with the CC leads to high standard deviations of the $\%_{CC-AM}$ average values, affecting the model accuracy.

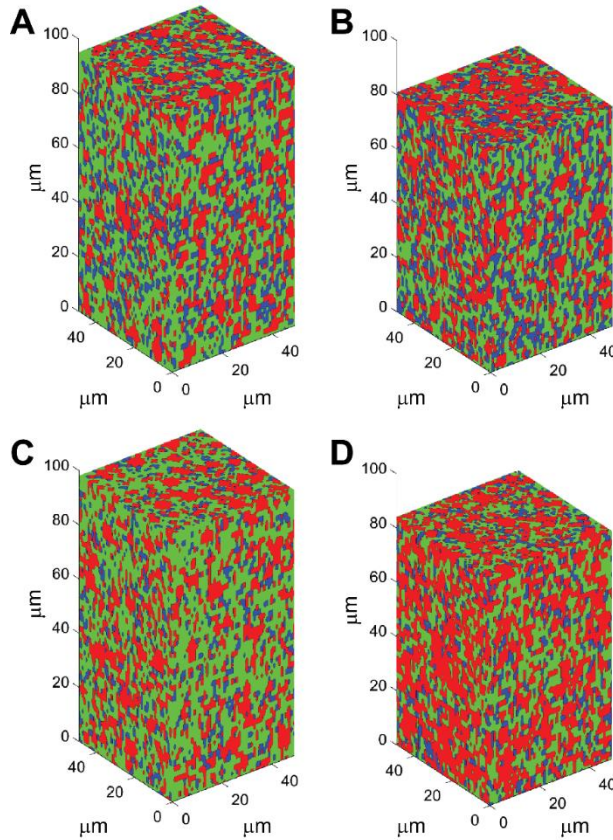


Figure 3. Examples of electrode mesostructures generated along this work with different AM-CBD compositions and ε_{cal} : 93-7 and 0.402 (A), 93-7 and 0.305 (B), 96-4 and 0.428 (C) and 96-4 and 0.33 (D). All the electrode mesostructures correspond to calendered electrodes with $\varepsilon_{init} = 0.48$. Red, blue and green pixels represent AM, CBD and electrolyte, respectively.

The ε_{init} analysed values ranged between 40% and 50%, the AM amount, between 93% and 96% and the calender pressure was varied between 20 and 170 MPa. The training+test datasets consisted in 440 data points, including all the electrode properties for different calendaring conditions (fully reported as text file in the Supporting Information), while the validation dataset contained other 440 data points not considered in both training and test sets. Each data point comes from the average properties of 10 generated electrode mesostructures. Consequently, 8800 electrode mesostructures were generated to build the training, test and validation datasets. Regarding the computational cost of the proposed procedure, the generation of the electrodes mesostructures and the analysis of their properties took approximately 7 days by using an Intel® Core™ i7-8700 CPU @ 3.2 GHz with 32 GB of RAM. Training the SISO models took approximately 24 hours by using 9 processors Intel® Xeon® CPU E5-2680 v4 @ 2.40 GHz, 128 GB of RAM.

2.2. Experimental methods

LiNi_{1/3}Mn_{1/3}Co_{1/3}O₂ (NMC) was supplied by Umicore. C-ENERGY™ super C65 carbon black (CB) was supplied by IMERYYS. Solef™ Polyvinylidene fluoride (PVdF) was purchased from Solvay and N-methylpyrrolidone (NMP), from BASF. The mass ratio between CB and binder was maintained equal to one. The slurry solid components NMC, CB and PVdF were premixed with a soft blender overnight. Afterwards, NMP was added until reaching the desired ratio between the solid components and the solvent (check Supporting Information, section S1a for further details). The mixture was performed in a Dispermat CV3-PLUS high-shear mixer for 2 h in a water-bath cooled recipient at 25 °C. The slurry was coated over a 22 µm thick Aluminium CC using a comma-coater prototype-grade machine (PDL250, People & Technology, Korea), fixing the gap at 300 µm and the coating speed at 0.3 m/s. The electrodes were dried in a built-in two-parts oven (one meter long each) at 80 and 95 °C and calendered with a prototype-grade lap press calender (BPN250, People & Technology, Korea). The latter consists in a two-roll compactor of 25

cm of diameter in which the gap between the rolls controls the pressure applied to the electrodes. Furthermore, both the roll speed and the roll temperature can be controlled. The calendaring was performed at various applied pressures and at constant line speed (0.54 m/min) and roll temperature (60 °C).

3. RESULT AND DISCUSSIONS

Our hybrid methodology was used to analyse the effect of the applied calender pressure (P) on the following electrode properties: (i) tortuosity (t) and electrolyte effective conductivity (σ_{eff}), (ii) percentage of current collector covered by AM or CBD particles, and (iii) active surface. Hereafter, the τ values correspond to the square root of the tortuosity factor.⁴⁵ All the results are analysed in terms of the electrode porosity before the calendaring ($\varepsilon_{\text{init}}$) and the electrode composition.

Figure 4 shows the ε_{cal} obtained through the experimental polynomial fitting in terms of the calender pressure applied for different $\varepsilon_{\text{init}}$ and AM compositions. At a given calendaring pressure, by increasing the AM amount, higher values of ε_{cal} are attained. The CB and polymer are located around AM particles, partly occupying the interstitial spaces of the AM network. As they are smaller respect AM particles, upon deformation due to calendaring, they occupy a higher fraction of the latter region, generating a more compact electrode.⁴⁶ On the other side, higher $\varepsilon_{\text{init}}$ values output lower porosities after calendaring, indicating that an initially more porous electrode would have more degrees of freedom to reorganize its structure upon an applied pressure, which leads to a more compact and interconnected solid phase network. This is of major importance for the electrode manufacturing process, as during the coating and drying stages the process parameters should be controlled to reach an optimal porosity. As we showed in our previous work,³² this can be modulated not only by the slurry AM/CB/binder relative composition but also with the amount of solvent used during the slurry preparation. In general, a sufficient

amount of the latter is needed for a proper dispersion of the solid particles, dissolution of the polymer and processability of the slurry during the coating stage.

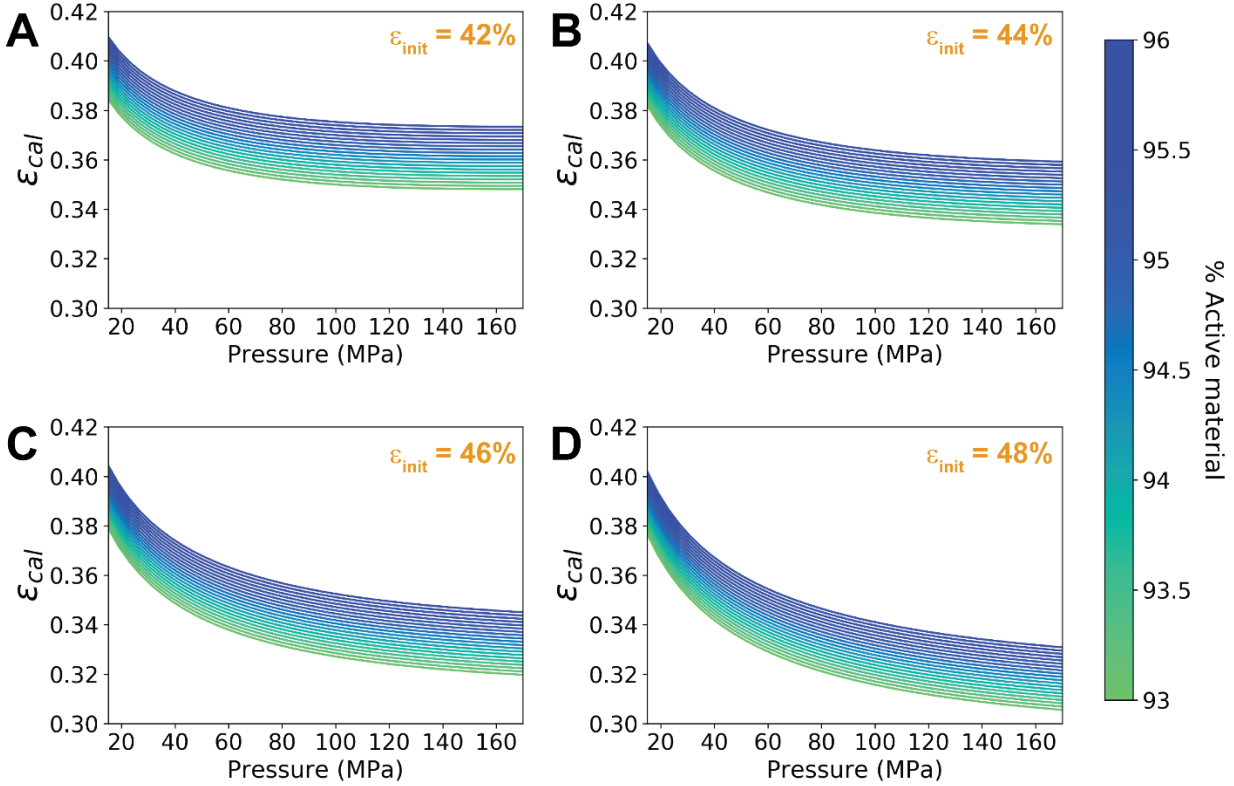


Figure 4. ϵ_{cal} obtained by polynomial fitting of the experimental dataset, in terms of the applied calender pressure and the AM mass fraction for different initial electrode porosities (ϵ_{init}): A) 42%, B) 44%, C) 46% and D) 48 %.

Figure 5 reports the ML-predicted solid tortuosity (τ_{sol}) as a function of the pressure applied during the calendaring for different ϵ_{init} and AM mass fractions. τ_{sol} is defined as the tortuosity associated to a generic particle moving through the particles network, without discrimination between AM and CBD phases. Consequently, it quantifies the interconnectivity of the particles network. τ_{sol} decreases by increasing the applied pressure, while the curves shift to higher values when the AM mass fraction grows. The effect of the former can be understood by considering that when applying a pressure, the volume fraction

of the solid phase and the contacts between particles increase, generating a bigger and more interconnected network that decreases τ_{sol} . On the other hand, as previously observed in Figure 4, incrementing the AM amount generates a less compact structure (higher ε_{cal}), leading to higher values of τ_{sol} . Furthermore, by comparing Figures 5 A, B, C and D the effect of ε_{init} on τ_{sol} can be analysed as well. Notably, lower τ_{sol} are reached at the lower ε_{cal} region, *i.e.* when increasing ε_{init} . As it was shown in Figure 4, higher ε_{init} output lower ε_{cal} , meaning more linear diffusion paths within the solid phase and less amount of constrictions and bottlenecks, making τ_{sol} to decrease.

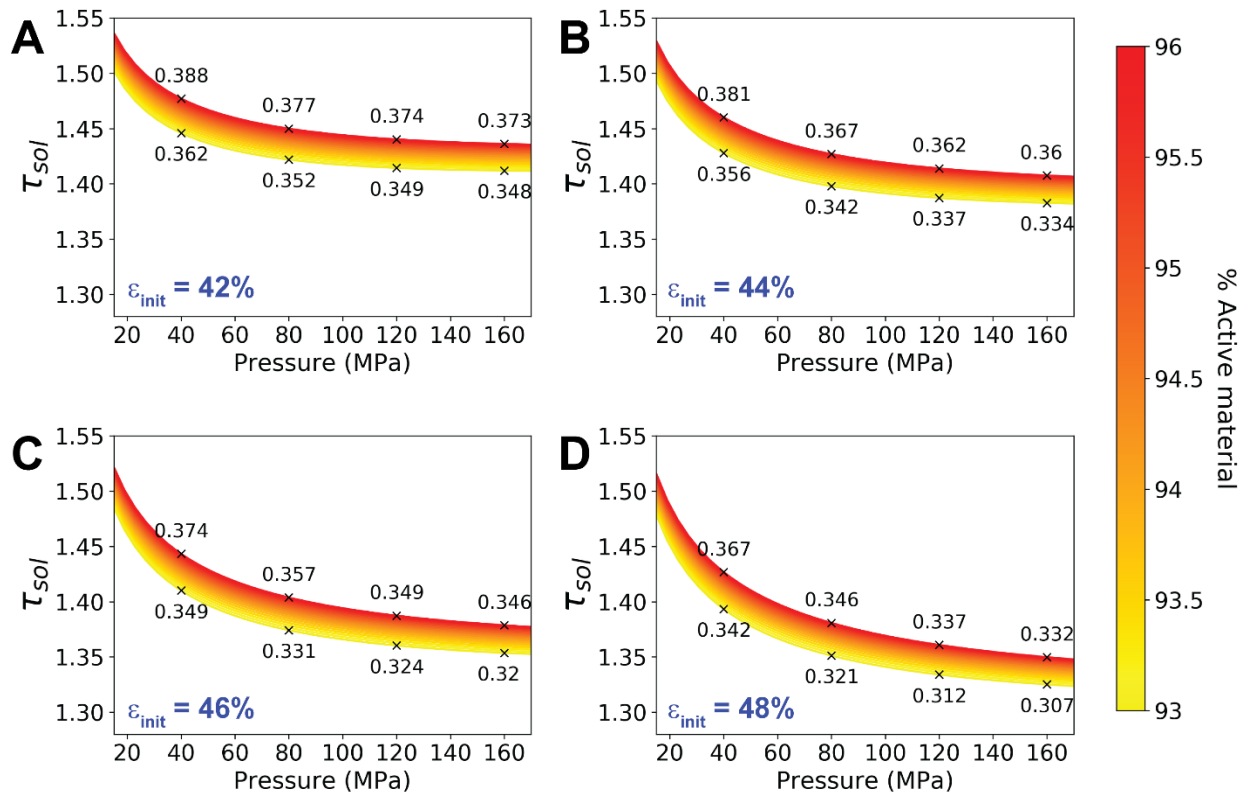


Figure 5. ML-predicted τ_{sol} in terms of the applied calender pressure and the AM mass fraction for different initial electrode porosities (ε_{init}): A) 42%, B) 44%, C) 46% and D) 48 %. For reference, the electrode porosity after the calendaring (ε_{cal}) are reported next to the cross symbols, for AM mass fractions equal to 93% and 96% at pressures equal to 40, 80, 120 and 160 MPa.

Figure 6 depicts the ML-predicted liquid tortuosity (τ_{liq}), *i.e.* the effective diffusivity of the Li^+ in the electrolyte through the porous medium, in terms of the pressure applied during the calendaring for different ε_{init} and AM mass fractions. It can be seen that τ_{liq} increases by incrementing the calender pressure. The latter is expected, as by increasing the applied pressure, ε_{cal} lowers, which reduces the size and interconnectivity of the pores. Moreover, the effect of pressure on τ_{liq} is more pronounced for lower amounts of AM and, consequently, higher amounts of CBD. Again, as the size of the CBD phase is smaller, upon reducing the porosity, it occupies the interstitial space between the bigger AM particles. This produces a drastic reduction in the size of AM interstitial pores when CBD mass fraction is higher, therefore outputting more tortuous paths within the pore phase. Moreover, it can be noticed that by increasing ε_{init} the effect of the pressure on τ_{liq} is even more accentuated, which leads to significantly higher values of τ_{liq} at high calendaring pressures. The latter is of particular relevance because it clearly indicates how the initial condition of the calendaring process can have a tremendous impact on the electrode properties arising from the manufacturing process itself. Lastly, it should be mentioned that the calculation of τ_{liq} performed with TauFactor does not take into account the microporosity of the CBD phase, which is expected to affect the results herein reported. Indeed, this would imply a higher volume fraction of smaller pores, leading to an even more marked increase of τ_{liq} for high-CBD-content electrodes (yellow curves in Figure 6).

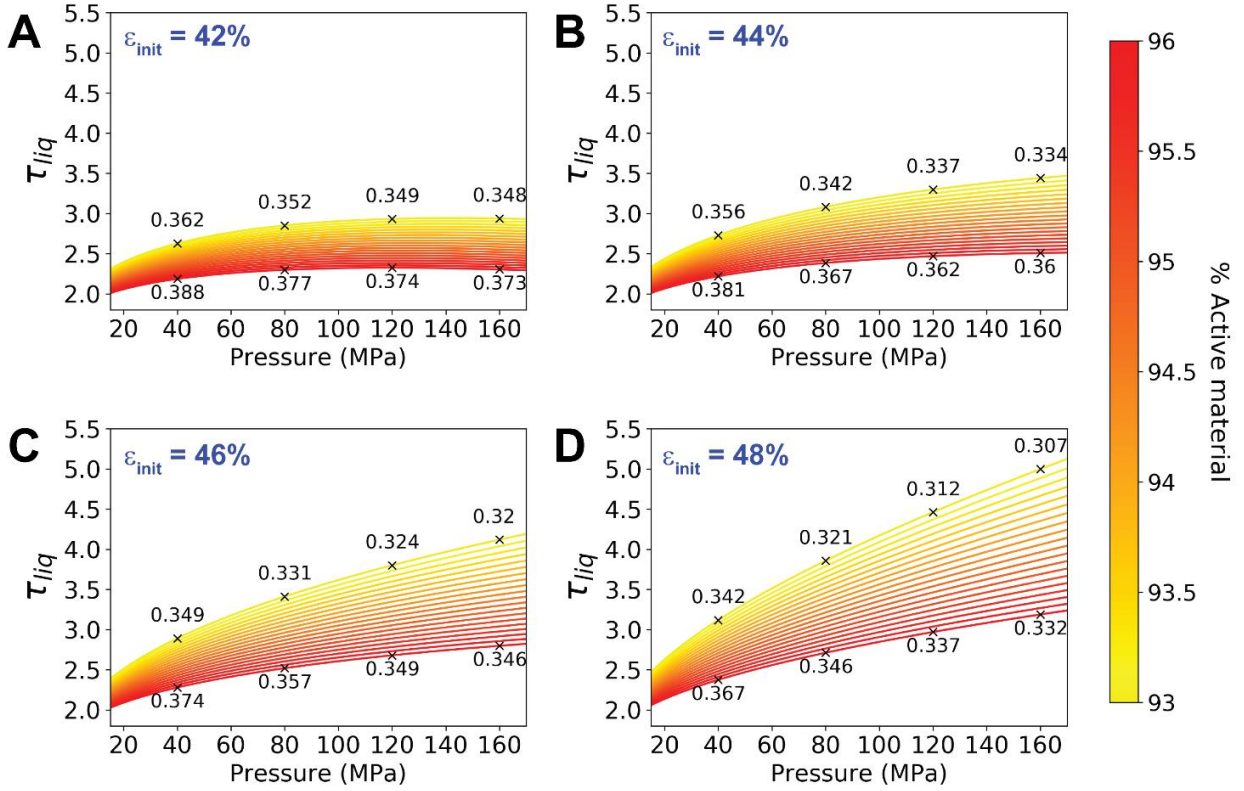


Figure 6. ML-predicted τ_{liq} in terms of the applied pressure and of the AM mass fraction for different initial electrode porosities (ϵ_{init}): A) 42%, B) 44%, C) 46% and D) 48 %. For reference, the electrode porosity after the calendaring (ϵ_{cal}) are reported next to the cross symbols, for AM mass fractions equal to 93% and 96% at pressures equal to 40, 80, 120 and 160 MPa.

τ_{liq} is also expected to affect the electrolyte effective ionic conductivity, which is a critical electrode property that impacts the LIB cell performance at high current densities/C-rates.⁴⁷ The relationship between these two features is captured by the MacMullin number (N_M)⁴⁸, which links the bulk and effective conductivity (σ_{bulk} and σ_{eff} , respectively) to the porosity and tortuosity factor (τ^2), as reported in Equation 1.

$$N_M = \frac{\sigma_{bulk}}{\sigma_{eff}} = \frac{\tau^2}{\epsilon} \quad (Eq. 1)$$

Taking into account that τ_{liq} and ε_{cal} have already been calculated for all the calendaring conditions/electrode initial properties here analysed, the σ_{eff} can be derived by using a reference σ_{bulk} . In this case, the σ_{bulk} used (1.119 S/m) comes from a commercial LP30 electrolyte, at 25 °C.⁴⁹ Furthermore, the analysis in terms of σ_{eff} allows to capture simultaneously the effect of both τ_{liq} and ε_{cal} .

Figure 7 shows the so calculated σ_{eff} as a function of ε_{cal} for different ε_{init} and AM mass fractions. For completeness, σ_{eff} plotted in terms of the applied calender pressure is presented in Figure S7, in the Supporting Information. Naturally, σ_{eff} decreases by reducing the electrode porosity while, at constant ε_{cal} , the higher the CBD content the lower σ_{eff} . This proves that not only the porosity value plays a key role in the electrolyte conductivity, but also the pore size distribution: smaller pores will cause a steeper reduction in σ_{eff} . By comparing the four panels, it can be seen that upon increasing ε_{init} lower σ_{eff} values are attained, as a consequence of the reduction in the minimal ε_{cal} that can be reached during the calendaring process. In this sense, the interdependency between the previous manufacturing stages and the output of the calendaring process are once again stressed, meaning that to control the impact of the latter on the electrolyte effective properties one should optimize the AM/CB/binder/solvent proportions and their impact on the electrode porosity after the drying step. Furthermore, as it has been acknowledged,^{31,50} there is a trade-off between σ_{eff} and the electrode electronic conductivity (somehow related to τ_{sol} , Figure 5): they should be both maximized upon calendaring. As by increasing the applied calender pressure the former gets reduced, the optimal ε_{cal} comes from a complex interplay between these two electrode properties.

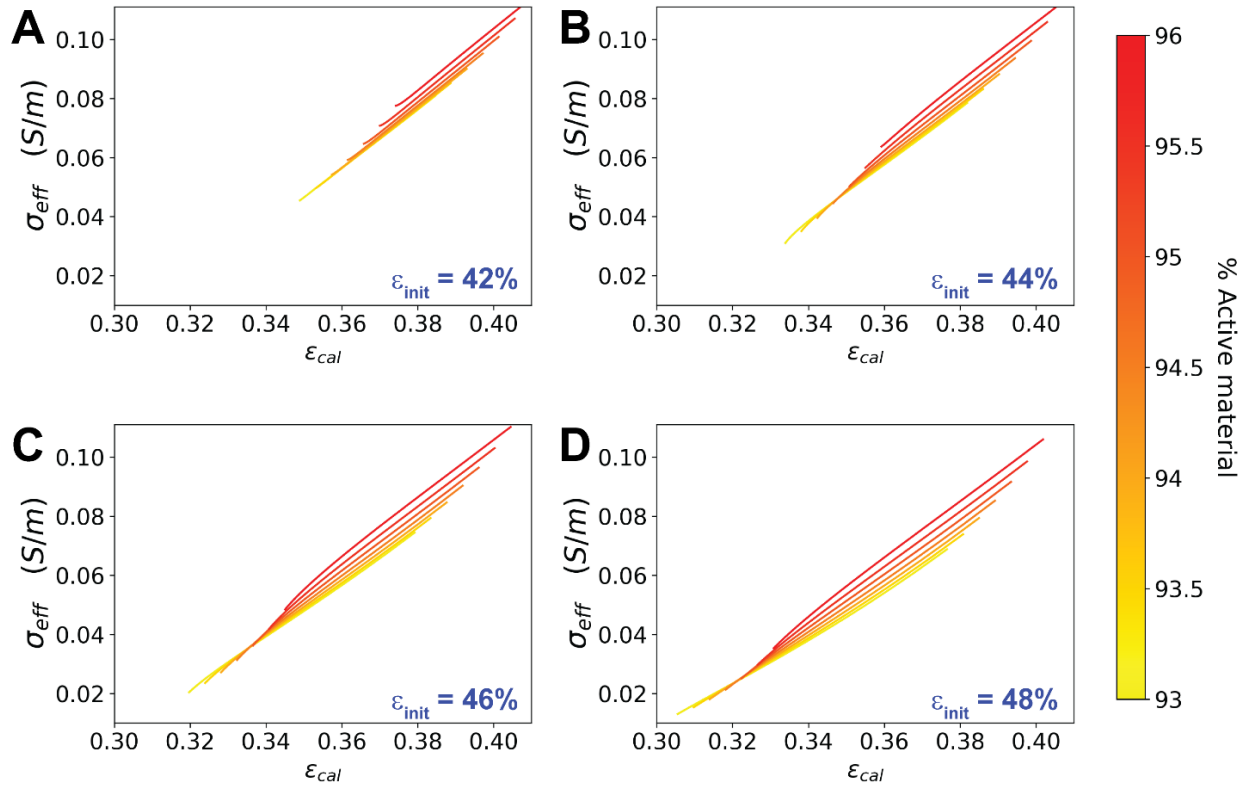


Figure 7. σ_{eff} in terms of the ϵ_{cal} and of the AM mass fraction for different initial electrode porosities (ϵ_{init}): A) 42%, B) 44%, C) 46% and D) 48 %.

One of the biggest advantages of our simulation approach is the ability to quantify mesoscale features completely inaccessible from the experimental point of view. One of them is the contacts between the solid phase and the CC, which is closely related to the adhesion strength and contact resistance of the electrode, and is modulated by the calendering process.^{51,52} Figure 8 shows the ML-predicted $\%_{CC-CBD}$, *i.e.* the percentage of current collector surface covered by the CBD phase, based on the pressure applied during the calendering for different ϵ_{init} and AM mass fractions. In the same way, Figure S8 in the Supporting Information displays $\%_{CC-AM}$. Remarkably, $\%_{CC-CBD}$ is only slightly influenced by ϵ_{init} , indicating that the increase in the electrode compactness arising from high ϵ_{init} does not significantly affect the CC coverage by the CBD phase. Moreover, increasing the calendering pressure leads to an increment of $\%_{CC-CBD}$ for low pressure

values, while for higher pressures it approaches to an asymptotic value being the latter slightly higher for higher ϵ_{init} . As expected, the increment in the CBD amount results in an increase of %_{CC-CBD}.

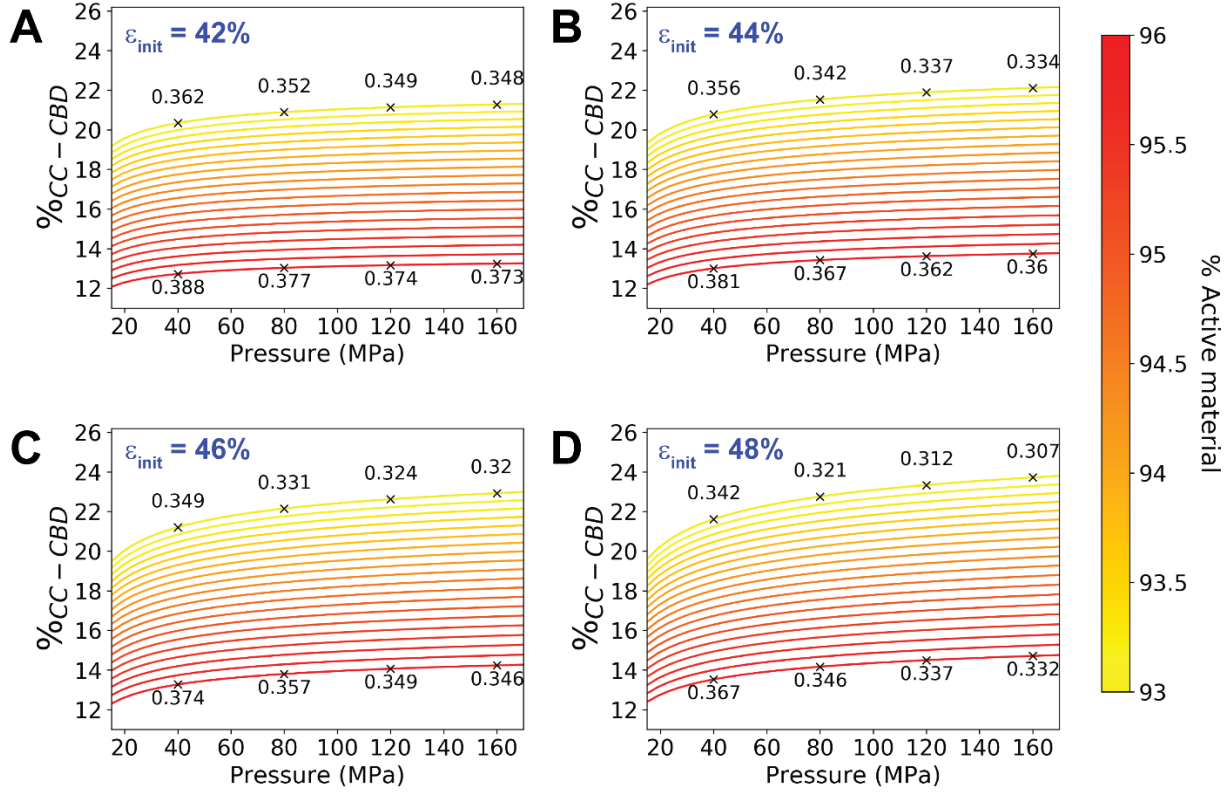


Figure 8. ML-predicted %_{CC-CBD} in terms of the pressure applied during the calendaring and of the AM mass fraction for different initial electrode porosities (ϵ_{init}): A) 42%, B) 44%, C) 46% and D) 48 %. For reference, the electrode porosity after the calendaring (ϵ_{cal}) are reported next to the cross symbols, for AM mass fractions equal to 93% and 96% at pressures equal to 40, 80, 120 and 160 MPa.

Another important mesoscale electrode property is the area of AM phase in contact with the electrolyte (AS), as this feature determines the effective Li^+ reaction rate in kinetic limited conditions (*i.e.* high current density operation conditions).^{27,31} In this sense, Figure 9 displays the ML-predicted AS based on the pressure applied during the calendaring, for different ϵ_{init} and AM mass fractions. As expected, by incrementing the AM amount, AS increases. Moreover, high values of ϵ_{init} leads to a decrease of AS, especially at high

pressure, due to the lower attainable ε_{cal} . Although we previously showed that higher ε_{init} are beneficial for attaining lower porosities (which would increase the volumetric energy/power density of the battery), this is detrimental in terms of AS, highlighting again that the optimal calendaring process condition must result from a compromise between several electrode properties.

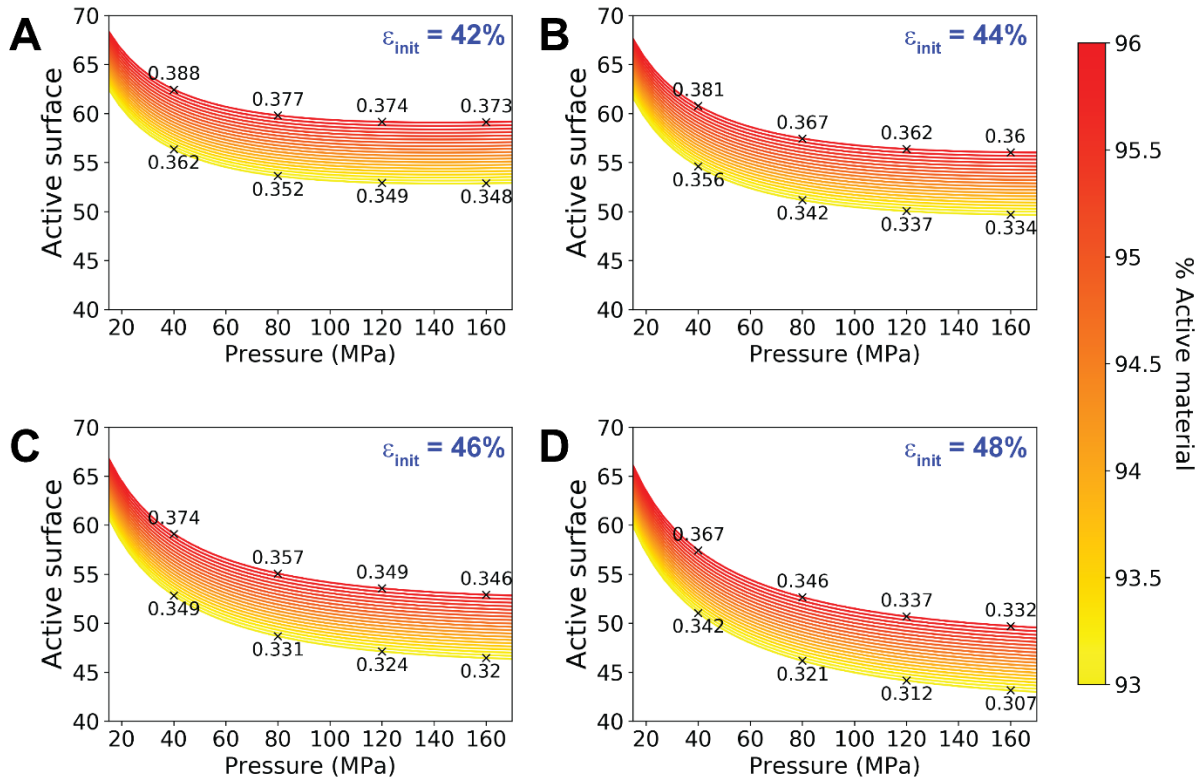


Figure 9. ML-predicted active surface in terms of the pressure applied during the calendaring and of the AM mass fraction for different initial electrode porosities (ε_{init}): A) 42%, B) 44%, C) 46% and D) 48 %. For reference, the electrode porosity after the calendaring (ε_{cal}) are reported next to the cross symbols, for AM mass fractions equal to 93% and 96% at pressures equal to 40, 80, 120 and 160 MPa.

Figure 10 summarizes the global trends found in this work by means of our ML-supported approach, where the colour of the circles (green/red) indicates if there is a direct or an inverse relationship between the variables, respectively. Furthermore, their size indicates the degree of correlation, meaning that bigger circles represent strongly correlated

variables, while smaller ones indicate that the output property is not significantly affected upon changing such initial condition. These interdependencies clearly reveal that the manufacturing optimization relies on a complex interplay of trade-offs. For example, the tortuosities of the liquid and solid phases have opposite relations with the initial electrode properties/process parameter, while both of them have to be minimized to improve the electrochemical performance. Similar remarks can be concluded for the AS and %_{CC-CBD}. In this case, both of them should be maximized while their correlations with the initial electrode properties/process parameter are opposites.

This correlation matrix also highlights the potential of tracking at a glance as many aspects as possible of the mesostructure evolution upon a manufacturing process such as the calendering, clearly indicating that it is not possible to find a general receipt to optimize LIB performance. The calendering pressure (and most likely all the electrode and process variables) should be tuned as a function of the electrode target performance. In this sense, the mathematical functions found along this work and reported explicitly in the Supporting Information could help manufacturers to identify the range of calender pressures, electrodes porosities prior the calendering and composition most suited for the application of interest, which is expected to accelerate the experimental manufacturing optimization.

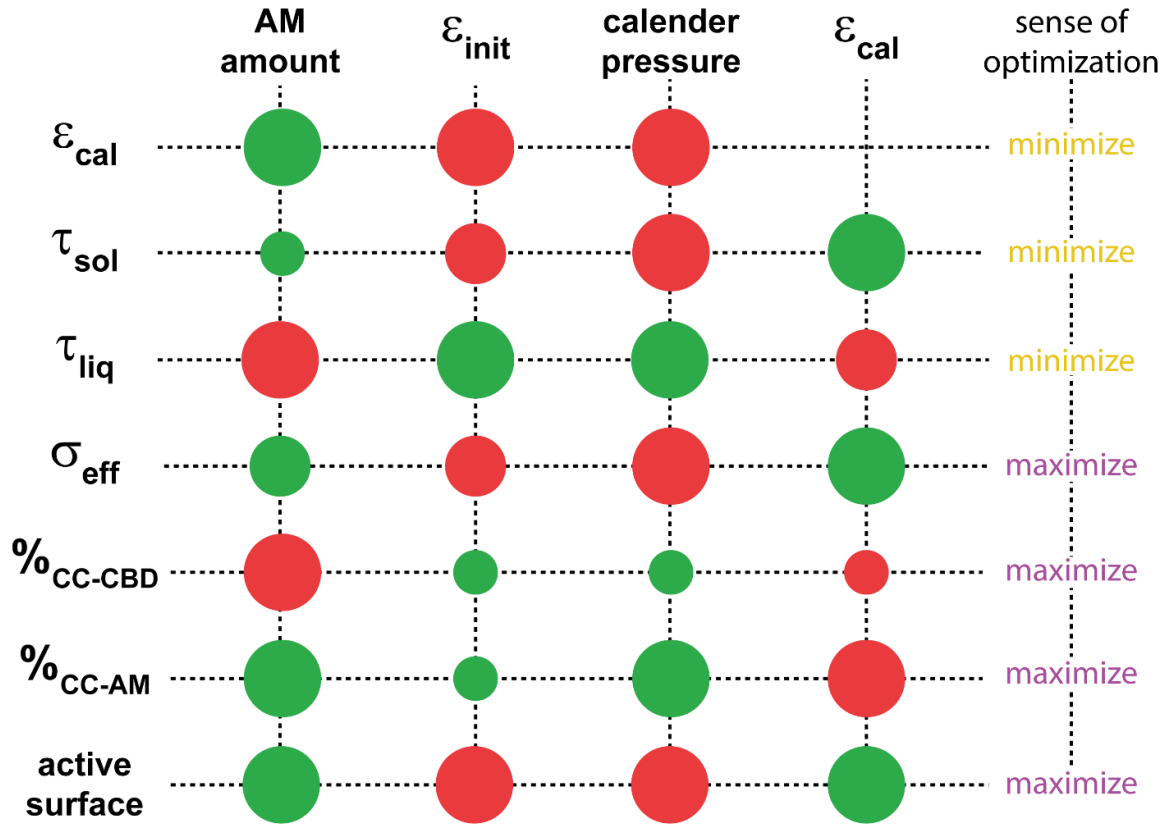


Figure 10. ML-assessed interdependencies between the calender pressure and the electrode properties before calendering and the output mesoscale properties. Green and red colours represent direct and inverse relations, respectively, while the size of the circles indicates the degree of correlation (*i.e.* big circles, strong correlation). The last column indicates the sense to which the property should be tuned (*i.e.* maximize or minimize the property) in order to increase an electrode performance descriptor (e.g. energy density).

What is more, the versatility of this methodology also ensures that by adding either more analysed properties or more physical details to the model, the results will be even more representative. Indeed, the changes in the volume fraction of the constituting phases were taken here as a metric to evaluate the effect of the applied calender pressure. Nonetheless, it is known that the electrode compression does not only impact the former but also causes particle deformation (or even breakage of the bigger AM particles),^{53,54} without overlooking the fact that mesostructural changes are expected to depend on how the CBD phase is

distributed throughout the electrode (tuned by the mixing and drying stages⁵⁵⁻⁵⁷). Further research to implement results coming from physics-based modelling, together with the experimental data, into the electrode mesostructure generating algorithm are ongoing and will be the core of further reports by our group. The latter will allow investigating manufacturing processes which are expected to influence mainly the particles reorganization along the electrode mesostructures, as for the case of solvent evaporation.⁵⁶ The chemical nature of the electrode components used and the AM or CBD particle size distribution can be other dimensions to further explore through this methodology.

4. Conclusions

This manuscript proposes a new hybrid methodology relying on the combined use of experimental and/or computational results capturing the influence of manufacturing parameters on the electrodes properties, a data-driven generator of electrode mesostructures and ML algorithms to ease the manufacturing parameters-electrode properties interdependencies analysis. Particularly, the new methodology was successfully applied to the case of NMC-based cathodes calendaring combining experimental results, *in silico* electrodes mesostructures and a ML algorithm based on the SISSO method. For the first time a single methodology allows to track the effect of the calender pressure, electrode composition and initial porosity on a wide array of mesoscale electrode properties critically influencing LIBs electrochemical performance. Specifically, the particle network interconnectivity, the electrolyte tortuosity and effective conductivity, the coverage of the current collector by CBD/AM particles and the active surface area were analysed and discussed in detail. The results obtained herein proved the validity and the potential of the proposed approach, clearly assessing the complexity of the interdependencies between manufacturing processes and electrode properties, paving the way to deeper understanding and then faster optimization. The need of tracking the effects of manufacturing on all the electrode properties impacting the electrochemical performance calls for novel optimization tools as the one proposed here, with the promise to ease and accelerate LIBs upgrades aiming to make feasible the electrical transition our society demands.

Author contributions

M.D. was in charge of the DNN and SISSO models development, the experimental data fitting and wrote Sections S1b, S4 and S5. T.L. was in charge of the writing and data analysis and supported the ML development. M.C. was in charge of the generation and analysis of the electrode mesostructures and wrote Section S3. E.N.P. was in charge of the experimental measurements and significantly supported the writing and data analysis. A.A.F. had the original idea of the hybrid concept proposed in this manuscript, supervised the project and the preparation of the manuscript and carried out its revision. All the authors contributed to the development of the concept behind this work.

Conflicts of interest

The authors declare no conflict of interest.

Acknowledgements

The authors acknowledge the European Union's Horizon 2020 research and innovation programme for the funding support through the European Research Council (grant agreement 772873, "ARTISTIC" project). A.A.F. acknowledges the Institut Universitaire de France for the support. M.D. and T.L. acknowledge Dr. Oier Arcelus from LRCS-Amiens (France) for very helpful discussions. The authors acknowledge Dr. Garima Shukla from LRCS-Amiens (France) for providing the experimental manufacturing schema reported in Figure 1A.

REFERENCES

- (1) Opitz, A.; Badami, P.; Shen, L.; Vignarooban, K.; Kannan, A. M. Can Li-Ion Batteries Be the Panacea for Automotive Applications? *Renew. Sustain. Energy Rev.* **2017**, *68*, Part 1, 685–692. <https://doi.org/10.1016/j.rser.2016.10.019>.
- (2) Winter, M.; Barnett, B.; Xu, K. Before Li Ion Batteries. *Chem. Rev.* **2018**, *118* (23), 11433–11456. <https://doi.org/10.1021/acs.chemrev.8b00422>.
- (3) Larcher, D. & J.-M. T. Towards Greener and More Sustainable Batteries for Electrical Energy Storage. *Nat. Chem.* **2015**, *7* (January), 19–29. <https://doi.org/10.1038/NCHEM.2085>.

- (4) Nitta, N.; Wu, F.; Lee, J. T.; Yushin, G. Li-Ion Battery Materials: Present and Future. *Mater. Today* **2015**, *18* (5), 252–264. <https://doi.org/10.1016/j.mattod.2014.10.040>.
- (5) Blomgren, G. E. The Development and Future of Lithium Ion Batteries. *J. Electrochem. Soc.* **2017**, *164* (1), A5019–A5025. <https://doi.org/10.1149/2.0251701jes>.
- (6) Assat, G.; Tarascon, J. M. Fundamental Understanding and Practical Challenges of Anionic Redox Activity in Li-Ion Batteries. *Nat. Energy* **2018**, *3* (5), 373–386. <https://doi.org/10.1038/s41560-018-0097-0>.
- (7) <https://materialsproject.org/>.
- (8) Poizot, P.; Dolhem, F.; Gaubicher, J. Progress in All-Organic Rechargeable Batteries Using Cationic and Anionic Configurations: Toward Low-Cost and Greener Storage Solutions? *Curr. Opin. Electrochem.* **2018**, *9* (April), 70–80. <https://doi.org/10.1016/j.coelec.2018.04.003>.
- (9) Cheng, C.; Drummond, R.; Duncan, S. R.; Grant, P. S. Combining Composition Graded Positive and Negative Electrodes for Higher Performance Li-Ion Batteries. *J. Power Sources* **2020**, *448* (July), 227376. <https://doi.org/10.1016/j.jpowsour.2019.227376>.
- (10) Nadeina, A.; Rozier, P.; Seznec, V. Facile Synthesis of a Common Na-Ion Battery Cathode Material $\text{Na}_3\text{V}_2(\text{PO}_4)_2\text{F}_3$ by Spark Plasma Sintering. *Energy Technology*. 2020. <https://doi.org/10.1002/ente.201901304>.
- (11) Maurel, A.; Courty, M.; Fleutot, B.; Tortajada, H.; Prashantha, K.; Armand, M.; Grugeon, S.; Panier, S.; Dupont, L. Highly Loaded Graphite-Polylactic Acid Composite-Based Filaments for Lithium-Ion Battery Three-Dimensional Printing. *Chem. Mater.* **2018**, *30* (21), 7484–7493. <https://doi.org/10.1021/acs.chemmater.8b02062>.

- (12) Wood, D. L.; Li, J.; Daniel, C. Prospects for Reducing the Processing Cost of Lithium Ion Batteries. *J. Power Sources* **2015**, *275*, 234–242. <https://doi.org/10.1016/j.jpowsour.2014.11.019>.
- (13) Thomitzek, M.; Schmidt, O.; Röder, F.; Krewer, U.; Herrmann, C.; Thiede, S. Simulating Process-Product Interdependencies in Battery Production Systems. *Procedia CIRP* **2018**, *72*, 346–351. <https://doi.org/10.1016/j.procir.2018.03.056>.
- (14) Turetsky, A.; Thiede, S.; Thomitzek, M.; von Drachenfels, N.; Pape, T.; Herrmann, C. Toward Data-Driven Applications in Lithium-Ion Battery Cell Manufacturing. *Energy Technol.* **2019**, *1900136*, 1900136. <https://doi.org/10.1002/ente.201900136>.
- (15) Kremer, L. S.; Hoffmann, A.; Danner, T.; Hein, S.; Prifling, B.; Westhoff, D.; Dreer, C.; Latz, A.; Schmidt, V.; Wohlfahrt-Mehrens, M. Manufacturing Process for Improved Ultra-Thick Cathodes in High-Energy Lithium-Ion Batteries. *Energy Technology*. 2020. <https://doi.org/10.1002/ente.201900167>.
- (16) Jaiser, S.; Müller, M.; Baunach, M.; Bauer, W.; Scharfer, P.; Schabel, W. Investigation of Film Solidification and Binder Migration during Drying of Li-Ion Battery Anodes. *J. Power Sources* **2016**, *318*, 210–219. <https://doi.org/10.1016/j.jpowsour.2016.04.018>.
- (17) Zheng, H.; Tan, L.; Liu, G.; Song, X.; Battaglia, V. S. Calendering Effects on the Physical and Electrochemical Properties of $\text{Li}[\text{Ni}_{1/3}\text{Mn}_{1/3}\text{Co}_{1/3}]\text{O}_2$ Cathode. *J. Power Sources* **2012**, *208*, 52–57. <https://doi.org/10.1016/j.jpowsour.2012.02.001>.
- (18) Meyer, C.; Bockholt, H.; Haselrieder, W.; Kwade, A. Characterization of the Calendering Process for Compaction of Electrodes for Lithium-Ion Batteries. *J. Mater. Process. Technol.* **2017**, *249* (November 2016), 172–178.

<https://doi.org/10.1016/j.jmatprotec.2017.05.031>.

- (19) Liu, Z.; Mukherjee, P. P. Microstructure Evolution in Lithium-Ion Battery Electrode Processing. *J. Electrochem. Soc.* **2014**, *161* (8), E3248–E3258. <https://doi.org/10.1149/2.026408jes>.
- (20) Rynne, O.; Dubarry, M.; Molson, C.; Lepage, D.; Prébé, A.; Aymé-Perrot, D.; Rochefort, D.; Dollé, M. Designs of Experiments for Beginners—A Quick Start Guide for Application to Electrode Formulation. *Batteries* **2019**, *5* (4). <https://doi.org/10.3390/batteries5040072>.
- (21) Rynne, O.; Dubarry, M.; Molson, C.; Nicolas, E.; Lepage, D.; Prébé, A.; Aymé-Perrot, D.; Rochefort, D.; Dollé, M. Exploiting Materials to Their Full Potential, a Li-Ion Battery Electrode Formulation Optimization Study. *ACS Appl. Energy Mater.* **2020**. <https://doi.org/10.1021/acsaem.0c00015>.
- (22) Sangrós Giménez, C.; Schilde, C.; Froböse, L.; Ivanov, S.; Kwade, A. Mechanical, Electrical, and Ionic Behavior of Lithium-Ion Battery Electrodes via Discrete Element Method Simulations. *Energy Technol.* **2019**. <https://doi.org/10.1002/ente.201900180>.
- (23) Sangrós Giménez, C.; Finke, B.; Nowak, C.; Schilde, C.; Kwade, A. Structural and Mechanical Characterization of Lithium-Ion Battery Electrodes via DEM Simulations. *Adv. Powder Technol.* **2018**, *29* (10), 2312–2321. <https://doi.org/10.1016/j.apr.2018.05.014>.
- (24) Sangrós Giménez, C.; Finke, B.; Schilde, C.; Froböse, L.; Kwade, A. Numerical Simulation of the Behavior of Lithium-Ion Battery Electrodes during the Calendaring Process via the Discrete Element Method. *Powder Technol.* **2019**, *349*, 1–11. <https://doi.org/10.1016/j.powtec.2019.03.020>.
- (25) Franco, A. A.; Rucci, A.; Brandell, D.; Frayret, C.; Gaberscek, M.; Jankowski, P.;

- Johansson, P. Boosting Rechargeable Batteries R&D by Multiscale Modeling: Myth or Reality? *Chem. Rev.* **2019**, *119* (7), 4569–4627. <https://doi.org/10.1021/acs.chemrev.8b00239>.
- (26) Lombardo, T.; Hoock, J.; Primo, E.; Ngandjong, C.; Duquesnoy, M.; Franco, A. A. Accelerated Optimization Methods for Force-Field Parametrization in Battery Electrode Manufacturing Modeling. *Batter. Supercaps* **2020**. <https://doi.org/10.1002/batt.202000049>.
- (27) Chouchane, M.; Rucci, A.; Lombardo, T.; Ngandjong C., A.; Franco, A. A. Lithium Ion Battery Electrodes Predicted from Manufacturing Simulations: Assessing the Impact of the Carbon-Binder Spatial Location on the Electrochemical Performance. *J. Power Source* **2019**. <https://doi.org/https://doi.org/10.1016/j.jpowsour.2019.227285>.
- (28) Shodiev, A.; Primo, E. N.; Chouchane, M.; Lombardo, T.; Ngandjong, A. C.; Rucci, A.; Franco, A. A. 4D-Resolved Physical Model for Electrochemical Impedance Spectroscopy of $\text{Li}(\text{Ni}_{1-x-y}\text{Mn}_x\text{Co}_y)\text{O}_2$ -Based Cathodes in Symmetric Cells: Consequences in Tortuosity Calculations. *J. Power Sources* **2020**, No. 454, 227871. <https://doi.org/10.1016/j.jpowsour.2020.227871>.
- (29) Rucci, A.; Ngandjong, A. C.; Primo, E. N.; Maiza, M.; Franco, A. A. Tracking Variabilities in the Simulation of Lithium Ion Battery Electrode Fabrication and Its Impact on Electrochemical Performance. *Electrochim. Acta* **2019**, *312*, 168–178. <https://doi.org/https://doi.org/10.1016/j.electacta.2019.04.110>.
- (30) Ngandjong, A. C.; Rucci, A.; Maiza, M.; Shukla, G.; Vazquez-Arenas, J.; Franco, A. A. Multiscale Simulation Platform Linking Lithium Ion Battery Electrode Fabrication Process with Performance at the Cell Level. *J. Phys. Chem. Lett.* **2017**, *8* (23), 5966–5972.

<https://doi.org/10.1021/acs.jpcelett.7b02647>.

- (31) Ferraro, M. E.; Trembacki, B. L.; Brunini, V. E.; Noble, D. R.; Roberts, S. A. Electrode Mesoscale as a Collection of Particles: Coupled Electrochemical and Mechanical Analysis of NMC Cathodes. *J. Electrochem. Soc.* **2020**, *167* (1), 013543. <https://doi.org/10.1149/1945-7111/ab632b>.
- (32) Cunha, R. P.; Lombardo, T.; Primo, E. N.; Franco, A. A. Artificial Intelligence Investigation of NMC Cathode Manufacturing Parameters Interdependencies. *Batter. Supercaps* **2020**, *3* (1), 60–67. <https://doi.org/doi:10.1002/batt.201900135>.
- (33) Bao, J.; Murugesan, V.; Kamp, C. J.; Shao, Y.; Yan, L.; Wang, W. Machine Learning Coupled Multi-Scale Modeling for Redox Flow Batteries. *Adv. Theory Simulations* **2020**, *3* (2), 1–13. <https://doi.org/10.1002/adts.201900167>.
- (34) Chen, C.; Zuo, Y.; Ye, W.; Li, X.; Deng, Z.; Ong, S. P. A Critical Review of Machine Learning of Energy Materials. *Adv. Energy Mater.* **2020**, *1903242*, 1–36. <https://doi.org/10.1002/aenm.201903242>.
- (35) Severson, K. A.; Attia, P. M.; Jin, N.; Perkins, N.; Jiang, B.; Yang, Z.; Chen, M. H.; Aykol, M.; Herring, P. K.; Fraggedakis, D.; et al. Data-Driven Prediction of Battery Cycle Life before Capacity Degradation. *Nat. Energy* **2019**, *4* (5), 383–391. <https://doi.org/10.1038/s41560-019-0356-8>.
- (36) Petrich, L.; Westhoff, D.; Feinauer, J.; Finegan, D. P.; Daemi, S. R.; Shearing, P. R.; Schmidt, V. Crack Detection in Lithium-Ion Cells Using Machine Learning. *Comput. Mater. Sci.* **2017**, *136*, 297–305. <https://doi.org/10.1016/j.commatsci.2017.05.012>.
- (37) Li, S.; Li, J.; He, H.; Wang, H. Lithium-Ion Battery Modeling Based on Big Data. *Energy*

- Procedia* **2019**, *159*, 168–173. <https://doi.org/10.1016/j.egypro.2018.12.046>.
- (38) Takagishi, Y.; Yamanaka, T.; Yamaue, T. Machine Learning Approaches for Designing Mesoscale Structure of Li-Ion Battery Electrodes. *Batteries* **2019**, *5* (3). <https://doi.org/10.3390/batteries5030054>.
- (39) Chouchane, M.; Primo, E. N.; Franco, A. A. Mesoscale Effects in the Extraction of the Solid-State Lithium Diffusion Coefficient Values of Battery Active Materials: Physical Insights from 3D Modeling. *J. Phys. Chem. Lett.* **2020**, 2775–2780. <https://doi.org/10.1021/acs.jpcclett.0c00517>.
- (40) Gayon-Lombardo, A.; Mosser, L.; Brandon, N. P.; Cooper, S. J. Pores for Thought: The Use of Generative Adversarial Networks for the Stochastic Reconstruction of 3D Multi-Phase Electrode Microstructures with Periodic Boundaries. *arXiv* **2020**.
- (41) Cooper, S. J.; Bertei, A.; Shearing, P. R.; Kilner, J. A.; Brandon, N. P. TauFactor: An Open-Source Application for Calculating Tortuosity Factors from Tomographic Data. *SoftwareX* **2016**, *5*, 203–210. <https://doi.org/10.1016/j.softx.2016.09.002>.
- (42) Lee, S. G.; Jeon, D. H.; Kim, B. M.; Kang, J. H.; Kim, C.-J. Lattice Boltzmann Simulation for Electrolyte Transport in Porous Electrode of Lithium Ion Batteries. *J. Electrochem. Soc.* **2013**, *160* (4), H258–H265. <https://doi.org/10.1149/2.017306jes>.
- (43) Russell, S.; Norvig, P. *Artificial Intelligence A Modern Approach*, 3rd ed.; Pearson Education, Inc., 2010.
- (44) Ouyang, R.; Curtarolo, S.; Ahmetcik, E.; Scheffler, M.; Ghiringhelli, L. M. SISSO: A Compressed-Sensing Method for Identifying the Best Low-Dimensional Descriptor in an Immensity of Offered Candidates. *Phys. Rev. Mater.* **2018**, *2* (8), 1–11.

<https://doi.org/10.1103/PhysRevMaterials.2.083802>.

- (45) Epstein, N. On Tortuosity and the Tortuosity Factor in Flow and Diffusion through Porous Media. *Chem. Eng. Sci.* **1989**, *44* (3), 777–779. [https://doi.org/https://doi.org/10.1016/0009-2509\(89\)85053-5](https://doi.org/https://doi.org/10.1016/0009-2509(89)85053-5).
- (46) Meyer, C.; Weyhe, M.; Haselrieder, W.; Kwade, A. Heated Calendering of Cathodes for Lithium-Ion Batteries with Varied Carbon Black and Binder Contents. *Energy Technol.* **2020**, *8* (2), 1900175. <https://doi.org/10.1002/ente.201900175>.
- (47) Tjaden, B.; Brett, D. J. L.; Shearing, P. R. Tortuosity in Electrochemical Devices: A Review of Calculation Approaches. *Int. Mater. Rev.* **2018**, *63* (2), 47–67. <https://doi.org/10.1080/09506608.2016.1249995>.
- (48) MacMullin, R. B.; Muccini, G. A. Characteristics of Porous Beds and Structures. *AIChE J.* **1956**, *2* (3), 393–403. <https://doi.org/10.1002/aic.690020320>.
- (49) <https://en.solvionic.com/products/1m-lipf6-in-ec-dmc-1-1-vol.-99.9>.
- (50) Laue, V.; Röder, F.; Krewer, U. Joint Structural and Electrochemical Modeling: Impact of Porosity on Lithium-Ion Battery Performance. *Electrochim. Acta* **2019**, *314*, 20–31. <https://doi.org/https://doi.org/10.1016/j.electacta.2019.05.005>.
- (51) van Bommel, A.; Divigalpitiya, R. Effect of Calendering LiFePO₄ Electrodes. *J. Electrochem. Soc.* **2012**, *159* (11), A1791–A1795. <https://doi.org/10.1149/2.029211jes>.
- (52) Schreiner, D.; Oguntke, M.; Günther, T.; Reinhart, G. Modelling of the Calendering Process of NMC-622 Cathodes in Battery Production Analyzing Machine/Material–Process–Structure Correlations. *Energy Technol.* **2019**, *7* (11), 1900840. <https://doi.org/10.1002/ente.201900840>.

- (53) Stershic, A. J.; Simunovic, S.; Nanda, J. Modeling the Evolution of Lithium-Ion Particle Contact Distributions Using a Fabric Tensor Approach. *J. Power Sources* **2015**, *297*, 540–550. <https://doi.org/10.1016/j.jpowsour.2015.07.088>.
- (54) Song, J. H.; Kim, Y. J.; Kim, J.; Oh, S. M.; Yoon, S. Relationship between Particle Hardness of $\text{LiNi}_{1/3}\text{Co}_{1/3}\text{Mn}_{1/3}\text{O}_2$ and Its Electrochemical Stability at High Temperature. *Bull. Korean Chem. Soc.* **2016**, *37* (8), 1298–1304. <https://doi.org/10.1002/bkcs.10858>.
- (55) Mayer, J. K.; Almar, L.; Asylbekov, E.; Haselrieder, W.; Kwade, A.; Weber, A.; Nirschl, H. Influence of the Carbon Black Dispersing Process on the Microstructure and Performance of Li-Ion Battery Cathodes. *Energy Technol.* **2020**, *8* (2), 1900161. <https://doi.org/10.1002/ente.201900161>.
- (56) Bauer, W.; Nötzel, D.; Wenzel, V.; Nirschl, H. Influence of Dry Mixing and Distribution of Conductive Additives in Cathodes for Lithium Ion Batteries. *J. Power Sources* **2015**, *288*, 359–367. <https://doi.org/https://doi.org/10.1016/j.jpowsour.2015.04.081>.
- (57) Bockholt, H.; Haselrieder, W.; Kwade, A. Intensive Powder Mixing for Dry Dispersing of Carbon Black and Its Relevance for Lithium-Ion Battery Cathodes. *Powder Technol.* **2016**, *297*, 266–274. <https://doi.org/https://doi.org/10.1016/j.powtec.2016.04.011>.